Original Article

Evaluation of Preoperative Microvascular Invasion in Hepatocellular Carcinoma Through Multidimensional Parameter Combination Modeling Based on Gd-EOB-DTPA MRI

Han-Dan Zhang[1#], Xiao-Ming Li[1#], Yu-Han Zhang[1], Fang Hu[1], Liang Tan[2,3], Fang Wang[4], Yang Jing[4], Da-Jing Guo[5], Yang Xu[5], Xian-Ling Hu[6], Chen Liu[1*] and Jian Wang[1*]

[1]Department of Radiology, Southwest Hospital, Third Military Medical University (Army Military Medical University), Chongqing, China; [2]Department of Neurosurgery, Third Military Medical University (Army Military Medical University), Chongqing, China; [3]Department of Electrical and Computer Engineering, Faculty of Science and Technology, University of Macau, Macau, China; [4]Department of Market, Huiying Medical Technology Co., Ltd, Beijing, China; [5]Department of Radiology, The Second Affiliated Hospital of Chongqing Medical University, Chongqing, China; [6]Communication Sergeant School, Army Engineering University of PLA, Chongqing, China

Abstract

Background and Aims: The study established and compared the efficacy of the clinicoradiological model, radiomics model and clinicoradiological-radiomics hybrid model in predicting the microvascular invasion (MVI) of hepatocellular carcinoma (HCC) using gadolinium ethoxybenzyl diethylene triaminepentaacetic acid (Gd-EOB-DTPA) enhanced MRI. ***Methods:*** This was a study that enrolled 602 HCC patients from two institutions. Least absolute shrinkage and selection operator (Lasso) method was used to screen for the most important clinicoradiological and radiomics features that predict MVI pre-operatively. Three machine learning algorithms were used to establish the clinicoradiological, radiomics, and clinicoradiological-radiomics hybrid models. Area under the curve (AUC) of receiver operating characteristic (ROC) curves and Delong's test were used to compare and quantify the predictive performance of the models. ***Results:*** The AUCs of the clinicoradiological model in training and validation cohorts were 0.793 and 0.701, respectively. The radiomics signature of arterial phase (AP) images alone achieved satisfying predictive efficacy for MVI, with AUCs of 0.671 and 0.643 in training and validation cohort, respectively. The combination of clinicoradiological factors and fusion radiomics signature of AP and VP images achieved AUCs of 0.824 and 0.801 in training and validation cohorts, 0.812 and 0.805 in prospective validation and external validation cohorts, respectively. The hybrid model provided the best prediction results. The results of the Delong test revealed that there were statistically significant differences among the clinicoradiological-radiomics hybrid model, clinicoradiological model, and radiomics model (*p*<0.05). ***Conclusions:*** The combination of clinicoradiological factors and fusion radiomics signature of AP and VP images based on Gd-EOB-DTPA-enhanced MRI can effectively predict MVI.

Citation of this article: Zhang HD, Li XM, Zhang YH, Hu F, Tan L, Wang F, *et al*. Evaluation of Preoperative Microvascular Invasion in Hepatocellular Carcinoma Through Multidimensional Parameter Combination Modeling Based on Gd-EOB-DTPA MRI. J Clin Transl Hepatol 2023;11(2):350–359. doi: 10.14218/JCTH.2021.00546.

Introduction

Hepatocellular carcinoma (HCC) is one of the most common cancers worldwide and the third-leading cause of cancer-related death.[1,2] At present, surgical resection and liver transplantation are the first-line of HCC treatment, but the recurrence rates are still as high as 70% and 35%, respectively, in the 5 years after surgery.[3–5] Several studies have shown that microvascular invasion (MVI) is the main risk factor for early postoperative recurrence.[6] However, at present, MVI can only be diagnosed through invasive techniques such as surgery or histopathology of biopsy specimens. Accurate prediction of MVI before surgery will help in the development of treatment strategies, thereby improving the survival and quality of life of the patients.

Tumor size,[7–9] tumor margin, incomplete capsule,[2,10,11] and arterial peritumoral enhancement[12–14] are significantly associated with the occurrence of MVI. Observation of peritumoral hypointensity on hepatobiliary phase (HBP) 20 m
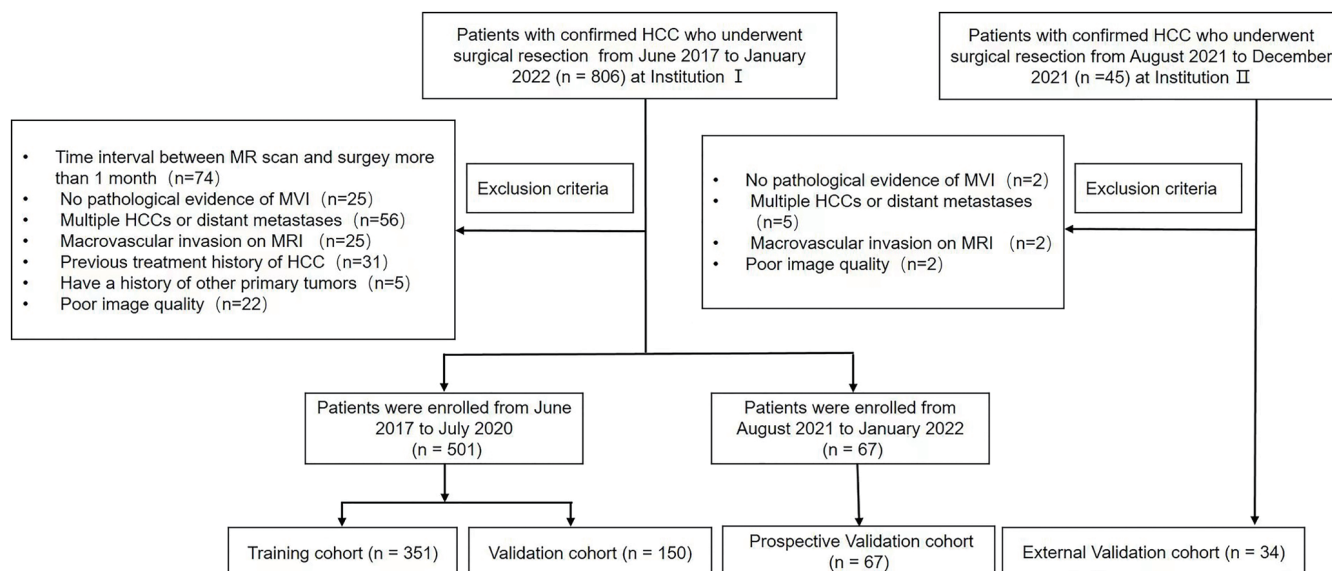
Fig. 1. Flowchart of patient inclusion. HCC, hepatocellular carcinoma; MRI, Magnetic Resonance Imaging; MVI, microvascular invasion.

after injection of the contrast agent gadolinium ethoxyben-zyl diethylenetriamine pentaacetic acid (Gd-EOB-DTPA) has become an important imaging feature for predicting MVI.[13,15] However, the imaging features are limited by many factors, including poor interobserver reproducibility and lack of external verification.[16] Radiomics is an emerging form of imaging analysis that uses a series of data-mining algorithms or statistical analysis tools to analyze high-throughput imaging features. Establishing appropriate models with quantitative features is important for predicting MVI.[17] Feng *et al*.,[18] Huang *et al*.,[19] and Peng *et al*.[1] demonstrated that the radiomics model is superior to arterial peritumoral enhancement, tumor margin, and peritumoral hypointensity on HBP in predicting MVI. However, there are other scholars who believe that radiomics is inferior to imaging features in predicting MVI. At present, the effectiveness of preoperative prediction of MVI using radiomics is still controversial, and there is need for further studies to support the reliability of radiomics. The purpose of this study was to establish and compare the efficacy of clinicoradiological model, a radiomics model, and a clinicoradiological-radiomics hybrid model based on Gd-EOB-DTPA-enhanced MRI in predicting MVI.

Methods

General clinical data

A group of 851 consecutive patients with HCC who underwent curative resection were recruited from June 2017 to January 2022 at two institutions. The written consents were obtained using protocols approved by Institutional Research Subpanel on Human Studies at Southwest Hospital. Based on the exclusion criteria listed in Figure 1, 501 patients who had visited Southwest Hospital between June 2017 and July 2020 were finally included in the study. The patients were randomly divided into training (351 cases) and validation (150 cases) cohorts at a ratio of 7:3. Sixty-seven HCC patients who had visited the hospital between August 2021 and January 2022 were included as a prospective validation cohort and 34 who had visited The Second Affiliated Hospital of Chongqing Medical University between August 2021

and December 2021 were included as an external validation cohort.

Clinical laboratory indicators and histopathology

Clinical data analyzed included sex, age, viral hepatitis B, and liver cirrhosis. Preoperative biochemical tests analyzed included AFP, white blood cell count, lymphocyte number, neutrophil number, platelet count, serum alkaline phosphatase, alanine aminotransferase, aspartate aminotransferase, serum albumin, serum total bilirubin, thrombin time, prothrombin time, and activated partial thromboplastin time (APTT).

The MVI status of all patients was evaluated by a pathologist with 15 years of working experience, who were blinded to other clinical information. MVI-positive was defined as the presence of cancer cell nests in the vascular cavity lined by endothelial cells under a microscope, with the branches of the portal vein, including intracapsular blood vessels, as the main branch, and no visible tumor vascular invasion.[20]

MRI

MRI examinations were performed using a 3.0T (TrioTim; Siemens Healthcare, Erlangen, Germany) and a 1.5T (Signa; GE, Milwaukee, Wisconsin, USA) MRI imaging system. Gd-EOB-DTPA at a dose of 0.1 mL/kg was injected through the cubital vein at a speed of 1.0 mL/s. The scan sequence before MRI enhancement included the positioning image, and the half-Fourier acquisition single-shot fast spin echo sequence (HASTE) coronary position, sagittal, chemical shift imaging, and three-dimensional volume interpolation rapid gradient echo (VIBE) plain scan. In the dynamic enhanced MRI scan, when the contrast agent reached the lower thoracic aorta, the patients held their breath for the arterial phase (AP) scan. The portal vein phase (VP), transitional phase and HBP scans were taken after a delay of 70 s, 2–5 m and 15 m. Diffusion weighted imaging (DWI) imaging adopted breathing-triggered single-shot echo planar imaging technology, with b values of 0, 400, and 800 s/mm². DWI uses spectral attenuation inversion recovery technol-

ogy for fat suppression. The apparent diffusion coefficient (ADC) value was calculated using a single exponential function with b values of 0 and 800 s/mm².

MRI evaluation

Picture archiving and communication system (PACS) was used to evaluate preoperative MRI images. Two radiologists (reader 1 and 2, with 8 years of experience in abdominal MRI diagnosis) independently reviewed all MRI images. Any discrepancies between the two radiologists were arbitrated by a senior physician with more than 10 years of abdominal diagnostic experience. The radiologists were aware of the diagnosis of HCC but were blinded to other clinical information. Inter-reader variation of imaging features was analyzed using k statistics. The imaging features evaluated included (1) tumor size, defined as the largest long axis on cross-sectional HBP image; (2) tumor margin, divided into smooth and non-smooth margins on the HBP image (a round or oval shape was considered to be smooth; irregularly lobulated tumors were considered non-smooth margins); (3) capsule, defined as a complete annular hyperenhancing structure at the tumor margin in the portal vein or transitional phase; (4) arterial peritumoral enhancement, defined as a crescent or polygonal enhancement around the tumor on the AP image, and the enhancement degree in the portal venous phase is slightly higher than or equal to that of the normal liver parenchyma; (5) peritumoral hypointensity on HBP, defined as a wedge-shaped or flame-shaped hypointensity around the hepatobiliary tumor; (6) intratumoral fat, defined as the presence of signal loss within the tumor in reverse phase sequence; (7) intratumoral hemorrhage, defined as a high signal in the tumor on the T1-weighted imaging (T1WI) sequence and a low signal on the susceptibility weighted imaging (SWI) sequence.

Image segmentation

The T1WI, T2WI, AP, VP, HBP, and ADC sequences of MRI for all patients were exported from the PACS system in DICOM format and uploaded to three-dimensional slicer software. Two radiologists (reader three, with 3 years of experience and reader four, with 4 years of experience in abdominal MRI diagnosis) manually segmented the tumor volume layer by layer on the six sequences, including the entire tumor, intratumoral hemorrhage, and necrotic areas, while avoiding abnormal peritumoral enhancement areas. The stability of each feature extracted from 30 randomly chosen patients was identified; reader three repeated the tumor segmentation twice within a week, and reader four performed the segmentation independently to assess intra- and inter-reader reproducibility. The reproducibility was subjected to intraclass correlation coefficient (ICC) analysis. Radiomics features with intra- and inter-reader ICC values greater than 0.75 indicated excellent stability and were selected for subsequent analysis.

Extraction and selection of radiomics features related to MVI

The original images and tumor segmentation images of T1WI, T2WI, AP, VP, HBP and ADC of 602 patients were uploaded to the Radcloud platform (Huiying Medical Technology Co., Ltd; Beijing, China), and 1,409 radiomic features were extracted for each sequence. The radiomics features were divided into the (1) intensity feature, which describes the intensity information of pixels in the region of inter-

est, including energy, entropy, means, standard deviations, variances, maxima, medians, ranges, and Kurtosis; (2) shape feature, which describes the shape and size of the area of interest, including volume, surface area, compactness, 2D/3D maximum diameter, and flatness; (3) texture features, which describe the relationship between pixels in the region of interest, that is, the texture information of the image, including the gray level co-occurrence matrix, the gray level dependence matrix, the gray level size zone matrix, the gray level run length matrix, and the sapient gray tone difference matrix; (4) high-order features, such as first-order features, and texture features, extracted after the image was subjected to filter transformation (i.e. logarithmic transformation, exponential transformation, and wavelet transformation).

Before the features were extracted, the platform automatically preprocessed the original image with the following parameters: resampled pixel spacing: (1,1,1), binwidth: 15, interpolator: SitkBSpline, and normalize: true. The normalization formula:

$$f(x) = \frac{s(x - \mu_x)}{\delta_x}$$

where x and f(x) are the pixel intensities of the original image and the standardized image, respectively, while μ_x and δ_x are the mean and standard deviation of the original image intensity values. To assess the ability of each individual MRI sequence to predict MVI, and to determine if combining different sequences improves MVI prediction, we performed correlation analyses of individual MRI sequences and the combination of different MRI sequences.

The nearZeroVar function was used to remove features with variance close to 0 and the ratio of the first mode to the second mode technique exceeding 0.95. To avoid multicollinearity, correlation coefficient analysis was used to delete features with correlation coefficients greater than 0.9. Finally, the Lasso algorithm was used to identify the final radiomics features that were most relevant in predicting MVI status. The Radscore of the corresponding MRI sequence was calculated according to the following formula:

$$Radscore = Intercept + \sum_{i-1}^{n} Coef_i \times Feature_i$$

where Intercept is the Lasso regression intercept, *n* is the total number of features screened by the Lasso algorithm, $Coef_i$ is the Lasso coefficient of the ith feature, and $Feature_i$ is the ith feature.

Screening of clinicoradiological risk factors

The classification index was examined using point-biserial analysis, continuous variables were evaluated by Pearson correlation analysis, and *t*-tests were used to evaluate the significance of correlations between clinicoradiological indicators and MVI status. The Lasso algorithm was used to determine potential risk factors for MVI.

Model establishment and evaluation

Logistic regression (LR, normwt: TRUE, penalty:0), random forest (RF, maxnodes: 2) and support vector machine (SVM, kernel: radial, cost: 1, gamma: 10) were used to establish the clinicoradiological model, radiomics model, and clinico-radiological-radiomics hybrid model for each MRI sequence and various combination sequences using R software. Receiver operating characteristic (ROC) curves were plotted, and area under the curve (AUC) was used determine the efficacy of MVI prediction. Comparison of ROC curves among

different models was performed using the Delong test and Bonferroni-corrected *p*-values and provided AUC, 95% confidence intervals (CIs), sensitivity, specificity, accuracy, and F1 values, quantitatively demonstrating model discriminant efficacy.

Statistical analysis

The statistical analysis was performed using R software (version 4.0.3; Boston, MA, USA). Continuous variables were reported as means (SD) and compared using *t*-tests. Qualitative variables were reported as counts and proportions and analyzed using chi-square tests. Two-tailed *p*-values <0.05 were considered statistically significant. In machine learning, clinicoradiological, radiomics, and hybrid models were developed using a training cohort (70%) to predict MVI status. A validation cohort (30%) was used to evaluate the generalization ability of models, and was quantitatively evaluated using AUC, accuracy, sensitivity, specificity, F1 value. Prospective and external validation cohorts were used to evaluate the generalization ability of hybrid model (Supplementary File 1).

Results

Clinicoradiological features

The agreement between the two radiologists for all imaging features was excellent (κ=0.75–0.79). Table 1 compares the clinical, laboratory, and imaging features of MVI-positive and negative patients in training, validation, prospective validation, and external validation cohorts. The results showed that AFP, APTT, tumor margin, size, capsule, intratumoral hemorrhage, arterial peritumoral enhancement and peritumoral hypointensity on HBP were significantly different between MVI-positive and MVI-negative groups (*p*<0.05) in training cohort. The Lasso algorithm identified AFP, APTT, tumor margin, capsule, intratumoral hemorrhage, arterial peritumoral enhancement and peritumoral hypointensity on HBP as important features affecting MVI (Fig. 2A).

Screening results of radiomics features

A total of 1,409 radiomics features were extracted from the volume of interest images of each MRI sequence. Variance threshold method, correlation coefficient analysis and Lasso algorithm were used for screening, and we found that 19 features in the best single sequence of AP, 18 features in the best fusion sequence of AP and HBP, and 18 features in the fusion sequence of AP and VP were the most important for predicting MVI (Fig. 2).

Establishment and evaluation of the prediction models

We established three prediction models in this study, clinicoradiological, radiomics, and clinicoradiological-radiomics hybrid models. The AUCs for predicting MVI using the clinicoradiological model based on AFP, APTT, tumor margin, capsule, intratumoral hemorrhage, arterial peritumoral enhancement and peritumoral hypointensity on HBP were 0.793 and 0.701 in the training and validation cohorts, respectively.

The best performing machine learning algorithm tested in

this study was achieved by RF. Table 2 shows the prediction performance of the single sequence and the optimal fusion sequence radiomics model. The results showed that AP had the best performance of the single sequence, with AUCs of 0.671 in training cohort and 0.643 in validation cohort. The fusion sequence with the best performance involved AP and HBP, with AUCs of 0.706 in training cohort and 0.625 in the cohort. These findings suggested that the single radiomics signature of AP had better predictive efficacy for MVI.

Comparison of the ROC curves of the three models showed that the clinicoradiological-radiomics hybrid model, which was the combination of clinicoradiological factors and fusion radiomics signature of AP and VP images, had the best predictive efficacy. The AUC of the model in training cohort was 0.824, and its sensitivity, specificity, and accuracy were 77.3%, 74.9%, and 76.1%, respectively. The AUC in validation cohort was 0.802, which was better than the radiomics model (AUCs 0.643 in validation cohort) and the clinicoradiological model (AUCs 0.701 in validation cohort). Furthermore, the AUCs were 0.812 and 0.805 in the prospective validation and external validation cohorts, respectively (Tables 2 and 3, and Fig. 3). The results of the Delong test revealed that the clinicoradiological-radiomics hybrid model was significantly different from the clinicoradiological and radiomics models (*p*<0.05).

Discussion

In this study, we showed that there were significant differences between the MVI-positive group and the MVI-negative group in AFP, APTT, tumor margin, size, capsule, intratumoral hemorrhage, arterial peritumoral enhancement, and peritumoral hypointensity on HBP (*p*<0.05). In addition to tumor size, the remaining seven features were very important in predicting MVI. An increase in serum AFP levels was associated with increased risk of MVI positivity, which was consistent with reports from literature.[21,22] High serum AFP levels are associated with high microvessel density, which increases the occurrence of MVI.[23] We also found that MVI-positive patients had prolonged APTT, which can be attributed to increased production of procoagulant activity factor (PCA) and proinflammatory cytokines by MVI-positive tumor cells and has not been reported in previous studies. PCA can activate the coagulation system and lead to the consumption of coagulation factors that leaves the body in a pre-bleeding state; while proinflammatory cytokines, including tumor necrosis factor-α and interleukin-1β, can reduce the activation of the protein-C system and promote intrinsic coagulation[24] leading to prolonged APTT.

Previous studies have shown that rough tumor margins,[12,13] incomplete capsule,[2,10,11] arterial peritumoral enhancement, and peritumoral hypointensity on HBP[12,13] are important risk factors for MVI, which is consistent with our findings. Those imaging features are associated with tumor malignant biological behavior. The tumor breaks through the capsule or infiltrates the adjacent liver parenchyma, and easily invades the peritumoral portal vein branches, resulting in compensatory blood supply of the peritumoral arterial branches. That causes a corresponding decrease in liver parenchyma function causing the dysfunctional hepatocytes around the tumor in the hepatobiliary stage to take up the contrast agent and emit a lower signal. The larger the tumor, the greater its heterogeneity, which may reflect underlying poor cellular differentiation with necrosis, angiogenesis, and extracellular matrix deposition. We also found that intratumoral hemorrhage was an important imaging feature for predicting MVI that had not previously been reported in literature. The possible mechanism is that the release of red blood cells and the aggregation of platelets after intra-

Table 1. Baseline patient characteristics

Characteristics	Training cohort (n=301)			Validation cohort (n=150)		
	MVI (−)	MVI (+)	P value	MVI (−)	MVI (+)	P value
	176	175		74	76	
Demographic data						
Sex			0.356			0.516
Male	148 (84.1)	154 (88.0)		60 (81.1)	65 (85.5)	
Female	28 (15.9)	21 (12.0)		14 (18.9)	11 (14.5)	
Age	53.34 (10.49)	50.61 (11.01)	0.18	52.88 (10.30)	51.70 (11.18)	0.502
Viral hepatitis B			0.103			0.81
Absent	27 (15.3)	16 (9.1)		10 (13.5)	9 (11.8)	
Present	149 (84.7)	159 (90.9)		64 (86.5)	67 (88.2)	
Cirrhosis			1			1
Absent	47 (26.7)	46 (26.3)		23 (31.1)	23 (30.3)	
Present	129 (73.3)	129 (73.7)		51 (68.9)	53 (69.7)	
Laboratory parameters						
AFP			0.007			0.612
Negative (0~20 ng/mL)	84 (47.7)	58 (33.1)		29 (39.2)	26 (34.2)	
Positive (>20 ng/mL)	92 (52.3)	117 (66.9)		45 (60.8)	50 (65.8)	
Neutrophils	6.45 (12.78)	5.19 (8.58)	0.278	5.42 (9.58)	5.66 (11.68)	0.892
WBC	5.97 (2.27)	6.01 (2.54)	0.891	5.75 (1.99)	5.96 (2.53)	0.57
Lymphocyte	9.53 (102.92)	1.54 (1.87)	0.305	1.57 (1.11)	1.46 (0.52)	0.404
Platelets	151.23(78.96)	159.89 (74.19)	0.291	153.35 (62.42)	154.17 (78.33)	0.944
ALP	119.15(113.4)	113.89 (71.57)	0.604	102.01 (30.58)	106.91 (67.79)	0.572
TBIL	18.86 (24.51)	18.20 (9.65)	0.74	17.68 (8.58)	17.79 (7.70)	0.932
ALB	42.04 (5.39)	41.88 (5.23)	0.782	41.64 (4.37)	42.11 (6.65)	0.611
ALT	59.90 (81.07)	74.00 (114.21)	0.183	59.93 (96.19)	50.16 (49.89)	0.435
AST	53.89 (69.58)	69.65 (99.41)	0.086	55.73 (78.39)	50.11 (39.00)	0.578
PT	13.56 (12.05)	12.15 (5.60)	0.16	14.42 (13.97)	11.44 (0.90)	0.066
TT	17.17 (1.35)	17.13 (1.74)	0.809	17.52 (1.33)	17.13 (1.51)	0.094
APTT	23.79 (10.19)	28.06 (3.81)	<0.001	30.79 (31.43)	28.28 (3.94)	0.49
Imaging features						
Intratumoral hemorrhage			<0.001			0.031
Absent	123 (69.9)	81 (46.3)		56 (75.7)	42 (55.3)	
Focal (<50%)	50 (28.4)	84 (48.0)		16 (21.6)	29 (38.2)	
Massive	3 (1.7)	10 (5.7)		2 (2.7)	5 (6.6)	
Intratumoral fat			0.468			0.644
Absent	148 (84.1)	147 (84.0)		63 (85.1)	65 (85.5)	
Focal (<50%)	19 (10.8)	23 (13.1)		8 (10.8)	10 (13.2)	
Massive	9 (5.1)	5 (2.9)		3 (4.1)	1 (1.3)	
Tumor margin			<0.001			<0.001
Smooth	110 (62.5)	37 (21.1)		44 (59.5)	18 (23.7)	
Not smooth	66 (37.5)	138 (78.9)		30 (40.5)	58 (76.3)	
Peritumoral hypointensity on hepatobiliary phase			<0.001			0.046
Absent	157 (89.2)	115 (65.7)		59 (79.7)	49 (64.5)	
Present	19 (10.8)	60 (34.3)		15 (20.3)	27 (35.5)	
Arterial peritumoral enhancement			<0.001			0.02
Absent	151 (85.8)	113 (64.6)		59 (79.7)	47 (61.8)	
Present	25 (14.2)	62 (35.4)		15 (20.3)	29 (38.2)	
Tumor size			<0.001			0.037
≤2 cm	32 (18.2)	18 (10.3)		17 (23.0)	7 (9.2)	
>2 and ≤3 cm	50 (28.4)	22 (12.6)		16 (21.6)	12 (15.8)	
>3 and ≤5 cm	59 (33.5)	55 (31.4)		24 (32.4)	27 (35.5)	
>5 cm	35 (19.9)	80 (45.7)		17 (23.0)	30 (39.5)	
Tumor capsule			<0.001			<0.001
Absent	12 (6.8)	24 (13.7)		6 (8.1)	9 (11.8)	
Complete	127 (72.2)	25 (14.3)		48 (64.9)	10 (13.2)	
Incomplete	37 (21.0)	126 (72.0)		20 (27.0)	57 (75.0)	

(extended)

Table 1. *(extended)*

Characteristics	Prospective Validation cohort (*n*=67)			External Validation cohort (*n*=34)		
	MVI (−)	MVI (+)	P	MVI (−)	MVI (+)	P
	31	36	value	24	10	value
Demographic data						
Sex			0.721			0.114
Male	22 (71.0)	28 (77.8)		20 (83.3)	5 (50.0)	
Female	9 (29.0)	8 (22.2)		4 (16.7)	5 (50.0)	
Age	52.55 (8.39)	52.53 (11.09)	0.993	53.00 (10.80)	59.20 (12.96)	0.16
Viral hepatitis B			1			0.18
Absent	5 (16.1)	5 (13.9)		3 (12.5)	4 (40.0)	
Present	26 (83.9)	31 (86.1)		21 (87.5)	6 (60.0)	
Cirrhosis			0.044			1
Absent	13 (41.9)	6 (16.7)		10 (41.7)	4 (40.0)	
Present	18 (58.1)	30 (83.3)		14 (58.3)	6 (60.0)	
Laboratory parameters						
AFP			0.57			0.363
Negative (0~20 ng/mL)	16 (51.6)	15 (41.7)		13 (54.2)	3 (30.0)	
Positive (>20 ng/mL)	15 (48.4)	21 (58.3)		11 (45.8)	7 (70.0)	
Neutrophils	3.22 (1.38)	3.41 (0.95)	0.518	4.27 (2.44)	2.98 (1.01)	0.119
WBC	5.03 (1.53)	5.18 (1.14)	0.646	6.39 (2.65)	4.89 (1.28)	0.099
Lymphocyte	1.37 (0.42)	1.67 (1.97)	0.414	1.44 (0.50)	1.36 (0.54)	0.709
Platelets	141.71 (52.08)	153.92 (62.39)	0.392	139.54 (43.76)	156.50 (66.38)	0.385
ALP	97.96 (31.62)	94.75 (28.68)	0.664	81.42 (20.38)	75.70 (30.38)	0.525
TBIL	15.04 (5.09)	18.41 (9.65)	0.085	11.74 (6.74)	10.40 (5.28)	0.581
ALB	43.88 (6.97)	43.00 (3.51)	0.505	41.90 (3.53)	40.36 (5.67)	0.341
ALT	37.29 (19.83)	37.75 (23.51)	0.931	28.62 (12.15)	38.10 (25.58)	0.149
AST	35.49 (16.27)	36.18 (15.67)	0.861	26.00 (6.31)	34.00 (14.85)	0.033
PT	11.15 (1.09)	11.24 (0.77)	0.713	13.65 (0.76)	13.32 (0.80)	0.272
TT	18.44 (1.11)	18.05 (1.07)	0.156	17.49 (1.12)	17.20 (1.28)	0.51
APTT	27.54 (2.00)	27.05 (2.12)	0.332	38.05 (4.49)	36.87 (2.26)	0.436
Imaging features						
Intratumoral hemorrhage			0.106			0.782
Absent	21 (67.7)	16 (44.4)		20 (83.3)	9 (90.0)	
Focal (<50%)	7 (22.6)	17 (47.2)		3 (12.5)	1 (10.0)	
Massive	3 (9.7)	3 (8.3)		1 (4.2)	0 (0.0)	
Intratumoral fat			0.785			0.026
Absent	23 (74.2)	27 (75.0)		18 (75.0)	5 (50.0)	
Focal (<50%)	5 (16.1)	7 (19.4)		1 (4.2)	4 (40.0)	
Massive	3 (9.7)	2 (5.6)		5 (20.8)	1 (10.0)	
Tumor margin			0.162			0.001
Smooth	24 (77.4)	21 (58.3)		21 (87.5)	2 (20.0)	
Not smooth	7 (22.6)	15 (41.7)		3 (12.5)	8 (80.0)	
Peritumoral hypointensity on hepatobiliary phase			<0.001			0.122
Absent	31 (100.0)	22 (61.1)		23 (95.8)	7 (70.0)	
Present	0 (0.0)	14 (38.9)		1 (4.2)	3 (30.0)	
Arterial peritumoral enhancement			<0.001			1
Absent	30 (96.8)	19 (52.8)		20 (83.3)	8 (80.0)	
Present	1 (3.2)	17 (47.2)		4 (16.7)	2 (20.0)	
Tumor size			0.65			0.059
≤2 cm	4 (12.9)	2 (5.6)		9 (37.5)	1 (10.0)	
>2 and ≤3 cm	9 (29.0)	10 (27.8)		8 (33.3)	1 (10.0)	
>3 and ≤5 cm	13 (41.9)	15 (41.7)		4 (16.7)	5 (50.0)	
>5 cm	5 (16.1)	9 (25.0)		3 (12.5)	3 (30.0)	
Tumor capsule			<0.001			0.015
Absent	2 (6.5)	8 (22.2)		3 (12.5)	1 (10.0)	
Complete	20 (64.5)	4 (11.1)		18 (75.0)	3 (30.0)	
Incomplete	9 (29.0)	24 (66.7)		3 (12.5)	6 (60.0)	

AFP, alpha-fetoprotein; ALB, serum albumin; ALP, serum alkaline phosphatase; ALT, alanine aminotransferase; APTT, activated partial thromboplastin time; AST, aspartate aminotransferase; PT, prothrombin time; TBIL, serum total bilirubin; TT, thrombin time; WBC, white blood cell count.
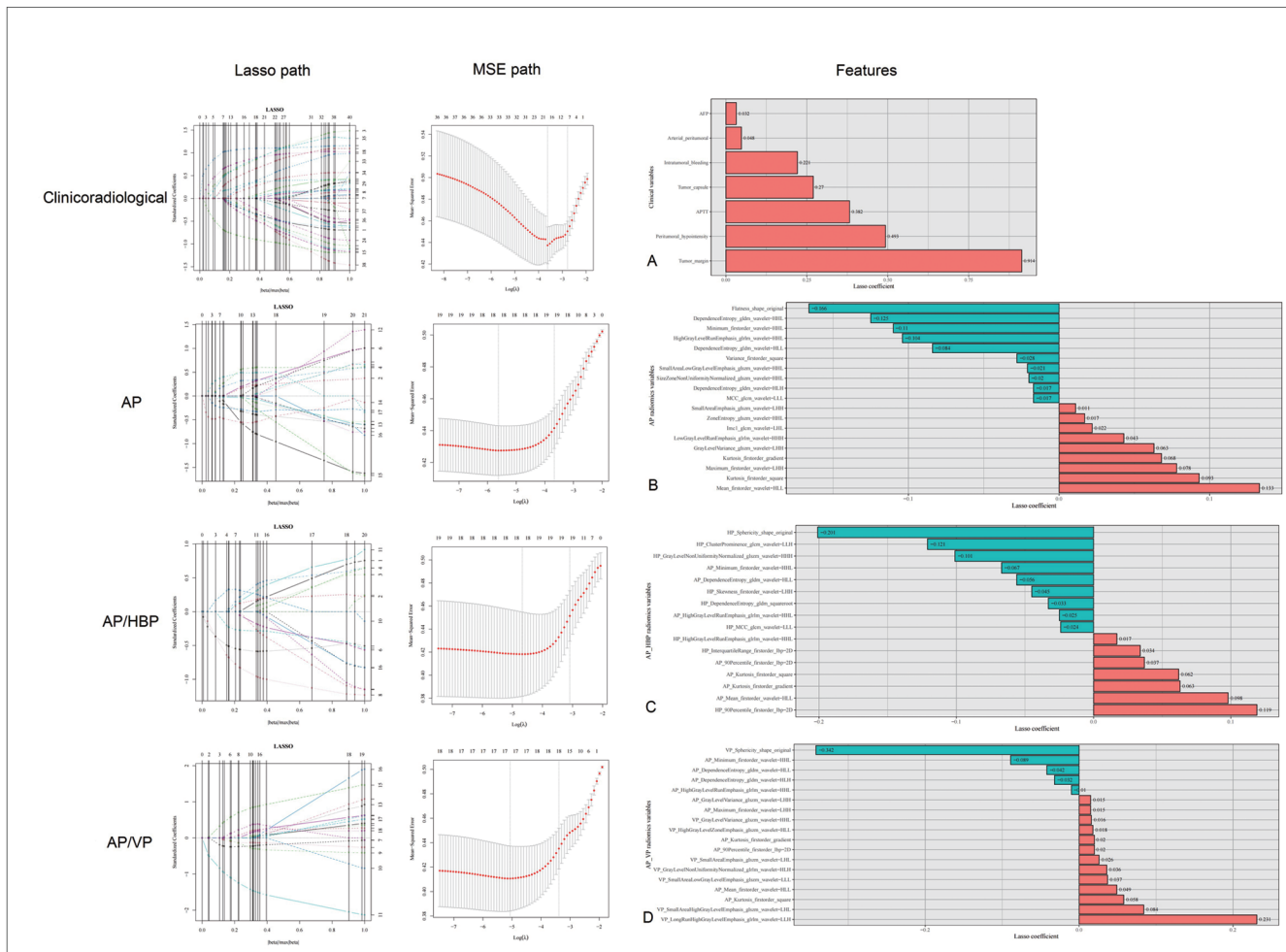
Fig. 2. Screening results of clinicoradiological and radiomics features. The left panels show the screening process of clinicoradiological and radiomics features based on the Lasso algorithm. The panels in the middle show the mean standard error of the Lasso algorithm during the clinicoradiological and radiomics feature screening process. The panels on the right show the clinicoradiological (A) and radiomics features, the AP sequence (B), the fusion sequence of AP and HBP (C), and the fusion sequence of AP and VP (D). AP, arterial phase; HBP, hepatobiliary phase; Lasso, least absolute shrinkage and selection operator; MSE, mean standard error; VP, portal vein phase.

tumoral hemorrhage activate the NF-kB pathway, thereby promoting tumor growth, invasion, and metastasis.[25] Yin *et al*.[26] also showed that extravascular erythrocytes and he-

moglobin can effectively promote tumor growth and tumor angiogenesis. For MVI-positive patients, liver transplantation and radiofrequency ablation are not recommended.[27-29]

Table 2. Performance of the single sequence and the optimal fusion sequence radiomics model

Se-quence	Training cohort						Validation cohort					
	AUC	CI	ACC	Sen	Spe	F1	AUC	CI	ACC	Sen	Spe	F1
T1WI	0.641	0.59–0.691	0.621	0.727	0.52	0.662	0.55	0.47–0.631	0.547	0.676	0.434	0.595
T2WI	0.673	0.618–0.727	0.632	0.631	0.646	0.641	0.566	0.49–0.643	0.493	0.797	0.355	NA
AP	0.671	0.617–0.726	0.615	0.716	0.531	0.628	0.643	0.559–0.727	0.58	0.324	0.895	0.636
VP	0.634	0.578–0.691	0.613	0.739	0.486	0.658	0.532	0.443–0.621	0.493	0.473	0.645	0.542
HBP	0.679	0.625–0.732	0.638	0.665	0.611	0.663	0.628	0.54–0.716	0.587	0.459	0.737	0.557
ADC	0.701	0.649–0.753	0.652	0.722	0.606	0.693	0.607	0.52–0.695	0.573	0.77	0.408	0.632
AP/HBP	0.706	0.652–0.759	0.658	0.631	0.686	0.649	0.625	0.537–0.714	0.567	0.284	0.934	0.575

NA indicated that the predictions of MVI-negative samples were wrong, resulting in confusion of the matrix of the prediction results and having only one row and two columns, so that precision value could not be calculated. F1=2 * (precision * sensitivity) / (precision + sensitivity); therefore, the F1 value is empty. ACC, accuracy; ADC, apparent diffusion coefficient; AP, arterial phase; AUC, area under the curve; CI, confidence interval; HBP, hepatobiliary phase; Sen, Sensitivity; Spe, Specificity; T1WI, T1-weighted imaging; T2WI, T2-weighted imaging; VP, portal vein phase.

Table 3. Predictive performance of the optimal clinicoradiological-radiomics hybrid model

Sequence	Evalua-tion factor	Training cohort			Validation cohort		
		Radiomics	Clinicora-diological	Hybrid	Radiomics	Clinicora-diological	Hybrid
AP/VP	AUC	0.659	0.793	0.824	0.572	0.701	0.802
	CI	0.603–0.714	0.748–0.838	0.781–0.866	0.482–0.663	0.619–0.783	0.732–0.872
	ACC	0.618	0.709	0.761	0.573	0.633	0.727
	Sensitivity	0.494	0.608	0.773	0.595	0.5	0.838
	Specificity	0.743	0.834	0.749	0.566	0.803	0.684
	F1	0.581	0.742	0.764	0.529	0.671	0.717

ACC, accuracy; AP, arterial phase; AUC, area under the curve; CI, confidence interval; VP, portal vein phase.
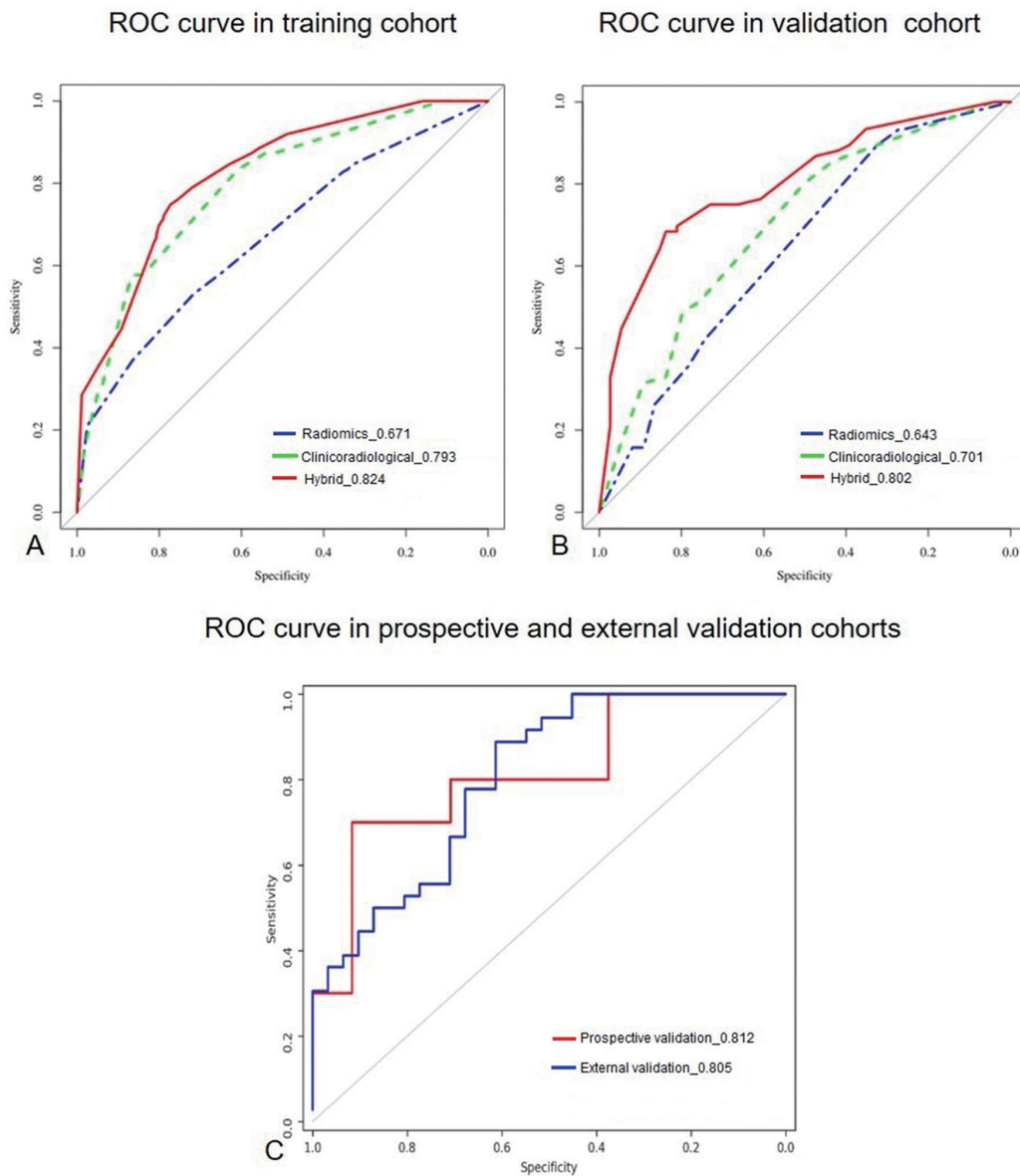

Fig. 3. Comparison of ROC curves for prediction of MVI. ROC curves of the clinicoradiological model, radiomics model of AP, and clinicoradiological-radiomics hybrid model that combines clinicoradiological factors and fusion radiomics signatures of AP and VP in training (A) and validation cohort (B). ROC curves of the clinico-radiological-radiomics hybrid model in prospective and external validation cohort (C). AP, arterial phase; ROC, receiver operating characteristic; VP, portal vein phase.

Patients with small HCC should undergo resection with a wider margin or anatomic resection, especially for lesions ≤2–3 cm, and for larger HCCs, anatomic resection was also associated with improved relapse-free survival (RFS).[30] In conclusion, wide margin resection can improve overall survival or RFS.

Several studies have reported that MRI radiomics can be used to predict MVI, but the radiomics features and their corresponding sequences that can effectively predict MVI are controversial and have poor reproducibility. A study by Nebbia *et al*.[31] on multiple sequences of T1WI, T2WI, DWI, AP and VP showed that single radiomics signature of T2WI and VP sequence achieved satisfying performance, with AUCs of 0.808 and 0.792 in the validation cohort, while the fusion radiomic signature of the two achieved the best performance, with AUCs of 0.867 in validation cohort. Zhang *et al*.[32] showed that the fusion radiomics signature of AP, VP, and DP achieved the best predictive efficacy for MVI. In this study, we found that single radiomics signature of AP performed better than any single or fusion sequence, which is consistent with the findings of Ma *et al*.[33] A possible reason is that radiomics signatures of different sequences are mutually exclusive, and the predictive performance of fusion radiomics signatures using multisequence performed worse. In addition, we found that radiomics signature achieved unsatisfactory predictive efficacy for MVI, with the AUC of the best prediction result being only 0.643 in validation cohort, which was significantly worse than the results reported in literature.[34,35] The discrepancy may be attributed to different inclusion criteria for tumors, scanning models, image acquisition times, and algorithms of artificial intelligence software.[17,36,37]

We established and compared the predictive efficacies of clinicoradiological, radiomics, and clinicoradiological-radiomics hybrid models to select the best preoperative method for predicting MVI, help in development of treatment strategies and prolong patient survival time. The results showed that the AUCs of the clinicoradiological model for predicting MVI were 0.793 and 0.701 in training and validation cohort, respectively. The AUCs of radiomics signature of AP were 0.671 and 0.643, respectively. The clinicoradiological-radiomics hybrid model, a combination of clinicoradiological factors and fusion radiomics signature of AP and VP images, had AUCs of 0.824 and 0.801 in the training and validation cohorts, and the AUCs were 0.812 and 0.805 in the prospective and external validation cohorts. We concluded that the combination of clinicoradiological factors and fusion radiomics signature of AP and VP images based on Gd-EOB-DTPA-enhanced MRI effectively predicted MVI status. We found that the performance of radiomics signature of AP or fusion radiomics signature of AP and HBP achieved better results than fusion radiomics signature of AP and VP, with AUCs of 0.643, 0.625 and 0.572 in validation cohort, respectively. However, the combination of clinicoradiological factors and radiomics signature of AP or the combination of clinicoradiological factors and fusion radiomics signature of AP and HBP had unsatisfactory prediction efficacy, with AUCs of 0.753 and 0.763 in validation cohort, respectively. The findings may have resulted from lack of significant differences in the performance of the radiomics signature of AP, fusion radiomics signature of AP and HBP or AP and VP. The respective predictive information of the clinicoradiological factors and fusion radiomics signature of AP and VP was just complementary, resulting in the combination of clinicoradiological factors and fusion radiomics signature of AP and VP achieving the best predictive efficacy, with AUCs of 0.802 in validation cohort.

In our study, the clinicoradiological model outperformed the radiomics signature, which is consistent with the results of Xu *et al*.,[17] who reported that the tumor capsule, margin, and arterial peritumoral enhancement are more important than radiomics R scores. However, several studies reported contrasting results. A meta-analysis by Huang *et al*.[19] revealed that the radiomic signature performed better than the clinicoradiological features. Feng *et al*.[18] found that the HBP radiomics signatures of 160 HCC patients outperformed imaging features such as arterial peritumoral enhancement, rough tumor margin, and peritumoral hypointensity on HBP, with AUCs of 0.57 in the validation cohort, which was consistent with the findings of Peng *et al*.[1] This inconsistency may be related to differences in population characteristics, or scan imaging and delineation methods. Research results with over-fitting, and poor reproducibility, also explain the difficulty in applying radiomics to clinical practice so far. In this study, the clinicoradiological-radiomics hybrid model achieved the best predictive efficacy, and the findings were consistent with Yang *et al*.[22] and Zhang *et al*.[32] Therefore, the radiomics model can be used as an auxiliary tool for clinicoradiological model to predict MVI.

The study has some limitations. First, the lesions were segmented manually, which may have had to poor reproducibility among investigators, and the results may not truly reflected the tumor margin characteristics There is need for validate our results using semi-automatic segmentation method. We also did not investigate whether peritumoral regional radiomics signatures have predictive value for MVI, which can be done in future studies.

Conclusions

The clinicoradiological model performed better than the radiomics model with Gd-EOB-DTPA enhanced MRI. The clinicoradiological-radiomics hybrid model had the best predictive efficacy for MVI.

Funding

Conflict of interest

The authors have no conflict of interests related to this publication.

Author contributions

Study conception and design (HDZ, XML, JW, CL), acquisition of data (HDZ, XML, YHZ, FH, DJG, YX), analysis and interpretation of data (HDZ, XML, FW, YJ, XLH), drafting of the manuscript (HDZ, XML), overall structure layout and language editing (LT), and critical revision of the manuscript for important intellectual content (JW, CL).

Data sharing statement

No additional data are available.

References

[1] Peng J, Zhang J, Zhang Q, Xu Y, Zhou J, Liu L. A radiomics nomogram for preoperative prediction of microvascular invasion risk in hepatitis B virus-related hepatocellular carcinoma. Diagn Interv Radiol 2018;24(3):121–127. doi:10.5152/dir.2018.17467, PMID:29770763.

[2]   Renzulli M, Biselli M, Brocchi S, Granito A, Vasuri F, Tovoli F, *et al*. New hallmark of hepatocellular carcinoma, early hepatocellular carcinoma and high-grade dysplastic nodules on Gd-EOB-DTPA MRI in patients with cirrhosis: a new diagnostic algorithm. Gut 2018;67(9):1674–1682. doi:10.1136/gutjnl-2017-315384, PMID:29437912.

[3]   Fong Y, Sun RL, Jarnagin W, Blumgart LH. An analysis of 412 cases of hepatocellular carcinoma at a Western center. Ann Surg 1999;229(6):790–799. doi:10.1097/00000658-199906000-00005, PMID:10363892.

[4]   Grazi GL, Ercolani G, Pierangeli F, Del Gaudio M, Cescon M, Cavallari A, *et al*. Improved results of liver resection for hepatocellular carcinoma on cirrhosis give the procedure added value. Ann Surg 2001;234(1):71–78. doi:10.1097/00000658-200107000-00011, PMID:11420485.

[5]   Lim K-C, Chow PK-H, Allen JC, Chia G-S, Lim M, Cheow P-C, *et al*. Microvascular Invasion Is a Better Predictor of Tumor Recurrence and Overall Survival Following Surgical Resection for Hepatocellular Carcinoma Compared to the Milan Criteria. Ann Surg 2011;254(1):108–113. doi:10.1097/SLA.0b013e31821ad884, PMID:21527845.

[6]   Renzulli M, Buonfiglioli F, Conti F, Brocchi S, Serio I, Foschi FG, *et al*. Imaging features of microvascular invasion in hepatocellular carcinoma developed after direct-acting antiviral therapy in HCV-related cirrhosis. Eur Radiol 2017;28(2):506–513. doi:10.1007/s00330-017-5033-3, PMID:28894901.

[7]   Pawlik TM, Delman KA, Vauthey JN, Nagorney DM, Ng IO, Ikai I, *et al*. Tumor size predicts vascular invasion and histologic grade: Implications for selection of surgical treatment for hepatocellular carcinoma. Liver Transpl 2005;11(9):1086–1092. doi:10.1002/lt.20472, PMID:16123959.

[8]   Kaibori M, Ishizaki M, Matsui K, Kwon AH. Predictors of microvascular invasion before hepatectomy for hepatocellular carcinoma. J Surg Oncol 2010;102(5):462–468. doi:10.1002/jso.21631, PMID:20872949.

[9]   Shirabe K, Toshima T, Kimura K, Yamashita Y, Ikeda T, Ikegami T, *et al*. New scoring system for prediction of microvascular invasion in patients with hepatocellular carcinoma. Liver Int 2014;34(6):937–941. doi:10.1111/liv.12459, PMID:24393295.

[10] Zhang L, Yu X, Wei W, Pan X, Lu L, Xia J, *et al*. Prediction of HCC microvascular invasion with gadobenate-enhanced MRI: correlation with pathology. Eur Radiol 2020;30(10):5327–5336. doi:10.1007/s00330-020-06895-6, PMID:32367417.

[11] Chou CT, Chen RC, Lee CW, Ko CJ, Wu HK, Chen YL. Prediction of microvascular invasion of hepatocellular carcinoma by pre-operative CT imaging. Br J Radiol 2012;85(1014):778–783. doi:10.1259/bjr/65897774, PMID:21828149.

[12] Renzulli M, Brocchi S, Cucchetti A, Mazzotti F, Mosconi C, Sportoletti C, *et al*. Can Current Preoperative Imaging Be Used to Detect Microvascular Invasion of Hepatocellular Carcinoma? Radiology 2016;279(2):432–442. doi:10.1148/radiol.2015150998, PMID:26653683.

[13] Lee S, Kim SH, Lee JE, Sinn DH, Park CK. Preoperative gadoxetic acid-enhanced MRI for predicting microvascular invasion in patients with single hepatocellular carcinoma. J Hepatol 2017;67(3):526–534. doi:10.1016/j.jhep.2017.04.024, PMID:28483680.

[14] Ahn SY, Lee JM, Joo I, Lee ES, Lee SJ, Cheon GJ, *et al*. Prediction of microvascular invasion of hepatocellular carcinoma using gadoxetic acid-enhanced MR and 18F-FDG PET/CT. Abdom Imaging 2014;40(4):843–851. doi:10.1007/s00261-014-0256-0, PMID:25253426.

[15] Kim KA, Kim MJ, Jeon HM, Kim KS, Choi JS, Ahn SH, *et al*. Prediction of microvascular invasion of hepatocellular carcinoma: usefulness of peritumoral hypointensity seen on gadoxetate disodium-enhanced hepatobiliary phase images. J Magn Reson Imaging 2012;35(3):629–634. doi:10.1002/jmri.22876, PMID:22069244.

[16] Zheng J, Chakraborty J, Chapman WC, Gerst S, Gonen M, Pak LM, *et al*. Preoperative Prediction of Microvascular Invasion in Hepatocellular Carcinoma Using Quantitative Image Analysis. J Am Coll Surg 2017;225(6):778–788. doi:10.1016/j.jamcollsurg.2017.09.003, PMID:28941728.

[17] Xu X, Zhang HL, Liu QP, Sun SW, Zhang J, Zhu FP, *et al*. Radiomic analysis of contrast-enhanced CT predicts microvascular invasion and outcome in hepatocellular carcinoma. J Hepatol 2019;70(6):1133–1144. doi:10.1016/j.jhep.2019.02.023, PMID:30876945.

[18] Feng ST, Jia Y, Liao B, Huang B, Zhou Q, Li X, *et al*. Preoperative prediction of microvascular invasion in hepatocellular cancer: a radiomics model using Gd-EOB-DTPA-enhanced MRI. Eur Radiol 2019;29(9):4648–4659. doi:10.1007/s00330-018-5935-8, PMID:30689032.

[19] Huang J, Tian W, Zhang L, Huang Q, Lin S, Ding Y, *et al*. Preoperative Prediction Power of Imaging Methods for Microvascular Invasion in Hepatocellular Carcinoma: A Systemic Review and Meta-Analysis. Front Oncol 2020;10(6):887. doi:10.3389/fonc.2020.00887, PMID:32676450.

[20] Zhou J, Sun H, Wang Z, Cong W, Wang J, Zeng M, *et al*. Guidelines for the Diagnosis and Treatment of Hepatocellular Carcinoma (2019 Edition). Liver Cancer 2020;9(6):682–720. doi:10.1159/000509424, PMID:33442540.

[21] Lei Z, Li J, Wu D, Xia Y, Wang Q, Si A, *et al*. Nomogram for Preoperative Estimation of Microvascular Invasion Risk in Hepatitis B Virus-Related Hepatocellular Carcinoma Within the Milan Criteria. JAMA Surg 2016;151(4):356–363. doi:10.1001/jamasurg.2015.4257, PMID:26579636.

[22] Yang L, Gu D, Wei J, Yang C, Rao S, Wang W, *et al*. A Radiomics Nomogram for Preoperative Prediction of Microvascular Invasion in Hepatocellular Carcinoma. Liver Cancer 2019;8(5):373–386. doi:10.1159/000494099, PMID:31768346.

[23] Li H, Li T, Hu J, Liu J. A nomogram to predict microvascular invasion in early hepatocellular carcinoma. J Cancer Res Ther 2021;17(3):652–657. doi:10.4103/jcrt.JCRT_1714_20, PMID:34269295.

[24] Wang XP, Mao MJ, He ZL, Zhang L, Chi PD, Su JR, *et al*. A retrospective discussion of the prognostic value of combining prothrombin time(PT) and fibrinogen(Fbg) in patients with Hepatocellular carcinoma. J Cancer 2017;8(11):2079–2087. doi:10.7150/jca.19181, PMID:28819409.

[25] Hu K, Wang ZM, Li JN, Zhang S, Xiao ZF, Tao YM. CLEC1B Expression and PD-L1 Expression Predict Clinical Outcome in Hepatocellular Carcinoma with Tumor Hemorrhage. Transl Oncol 2018;11(2):552–558. doi:10.1016/j.tranon.2018.02.010, PMID:29525632.

[26] Yin T, He S, Liu X, Jiang W, Ye T, Lin Z, *et al*. Extravascular red blood cells and hemoglobin promote tumor growth and therapeutic resistance as endogenous danger signals. J Immunol 2015;194(1):429–437. doi:10.4049/jimmunol.1400643, PMID:25429070.

[27] Lee S, Kang TW, Song KD, Lee MW, Rhim H, Lim HK, *et al*. Effect of Microvascular Invasion Risk on Early Recurrence of Hepatocellular Carcinoma After Surgery and Radiofrequency Ablation. Ann Surg 2021;273(3):564–571. doi:10.1097/SLA.0000000000003268, PMID:31058694.

[28] Aggarwal A, Te HS, Verna EC, Desai AP. A National Survey of Hepatocellular Carcinoma Surveillance Practices Following Liver Transplantation. Transplant Direct 2021;7(1):e638. doi:10.1097/TXD.0000000000001086, PMID:33324743.

[29] Nitta H, Allard MA, Sebagh M, Karam V, Ciacio O, Pittau G, *et al*. Predictive model for microvascular invasion of hepatocellular carcinoma among candidates for either hepatic resection or liver transplantation. Surgery 2019;165(6):1168–1175. doi:10.1016/j.surg.2019.01.012, PMID:30878140.

[30] Erstad DJ, Tanabe KK. Prognostic and Therapeutic Implications of Microvascular Invasion in Hepatocellular Carcinoma. Ann Surg Oncol 2019;26(5):1474–1493. doi:10.1245/s10434-019-07227-9, PMID:30788629.

[31] Nebbia G, Zhang Q, Arefan D, Zhao X, Wu S. Pre-operative Microvascular Invasion Prediction Using Multi-parametric Liver MRI Radiomics. J Digit Imaging 2020;33(6):1376–1386. doi:10.1007/s10278-020-00353-x, PMID:32495126.

[32] Zhang X, Ruan S, Xiao W, Shao J, Tian W, Liu W, *et al*. Contrast-enhanced CT radiomics for preoperative evaluation of microvascular invasion in hepatocellular carcinoma: A two-center study. Clin Transl Med 2020;10(2):e111. doi:10.1002/ctm2.111, PMID:32567245.

[33] Ma X, Wei J, Gu D, Zhu Y, Feng B, Liang M, *et al*. Preoperative radiomics nomogram for microvascular invasion prediction in hepatocellular carcinoma using contrast-enhanced CT. Eur Radiol 2019;29(7):3595–3605. doi:10.1007/s00330-018-5985-y, PMID:30770969.

[34] Zhang Y, Shu Z, Ye Q, Chen J, Zhong J, Jiang H, *et al*. Preoperative Prediction of Microvascular Invasion in Hepatocellular Carcinoma via Multi-Parametric MRI Radiomics. Front Oncol 2021;11(3):633596. doi:10.3389/fonc.2021.633596, PMID:33747956.

[35] Zhu YJ, Feng B, Wang S, Wang LM, Wu JF, Ma XH, *et al*. Model-based three-dimensional texture analysis of contrast-enhanced magnetic resonance imaging as a potential tool for preoperative prediction of microvascular invasion in hepatocellular carcinoma. Oncol Lett 2019;18(1):720–732. doi:10.3892/ol.2019.10378, PMID:31289547.

[36] He M, Zhang P, Ma X, He B, Fang C, Jia F. Radiomic Feature-Based Predictive Model for Microvascular Invasion in Patients With Hepatocellular Carcinoma. Front Oncol 2020;10(11):574228. doi:10.3389/fonc.2020.574228, PMID:33251138.

[37] Huang J, Tian W, Zhang L, Huang Q, Lin S, Ding Y, *et al*. Preoperative Prediction Power of Imaging Methods for Microvascular Invasion in Hepatocellular Carcinoma: A Systemic Review and Meta-Analysis. Front Oncol 2020;10(6):887. doi:10.3389/fonc.2020.00887, PMID:32676450.